



Regular Research Manuscript

Investigation of the Electrical Capacitance Tomography System for Determining the Spatial Distribution of Moisture in Grain Storage

Alfred J. Mwambela, and Shamte Kawambwa[†]

Department of Electronics and Telecommunication Engineering, University of Dar es Salaam,
Dar es Salaam, TANZANIA

[†]Corresponding author: shamtej2@gmail.com ORCID: 0000-0003-1937-8727

ABSTRACT

Excessive moisture content (MC) in stored grains promotes the growth of fungi and molds, which affects the quality of the grains. Effective grain monitoring methods are essential for detecting and managing grain spoilage. Electromagnetic imaging (EMI) techniques provide a promising alternative to traditional techniques by visualizing the spatial distribution of moisture within grains rather than merely average MC values offered by traditional techniques. However, existing EMI approaches often use hard-field waves, which are expensive and fragile. This study introduces an Electrical Capacitance Tomography (ECT) system that employs soft-field waves to monitor the moisture content of the grains. The system was calibrated against the oven-drying method to establish equations correlating MC with its voltage output. The system was adapted for image reconstruction using the Perspex materials of known shapes. Then, the ECT system was further adapted for spatial moisture visualization using two ECT image reconstruction algorithms. Results showed that the ECT system produced clear images of known shapes of Perspex materials and effectively visualized moisture distribution in grain samples within the sensor. The proposed approach represents a significant advancement in grain storage technology, offering a robust tool for improving grain monitoring and management practices.

ARTICLE INFO

Submitted: Sep. 30, 2024

Revised: Dec. 5, 2024

Accepted: Apr. 8, 2025

Published: Apr. 2025

Keywords: *Electrical Capacitance Tomography, Grain Moisture Contents, Grain Storage, Sensor Electronic, Linear Back Projection Algorithm.*

INTRODUCTION

Grain production involves several stages in the ecosystem, such as planting, processing, storage, and dissemination to the consumers. Grain storage plays a key role in the grain production cycle. The grain storage system preserves the quality of agricultural products, maintains the supply chain, balances between harvest and off seasons, controls the price in

the market, and preserves the grain species (Fu et al., 2024). The moisture content (MC) is among the most essential conditions influencing grain quality during storage. Moisture levels support the growth of microorganisms, which can cause mold, spoilage, and mycotoxin development, making grains unsafe for consumption (Leal et al., 2023; Lutz & Coradi, 2022). Low moisture levels can also negatively impact the

quality, making cracked grains more vulnerable to damage during handling and transportation. Maintaining such a hygroscopic balance in grain storage is desirable for preserving the quality of grains. The hygroscopic balance can be achieved through MC monitoring and subsequent control interventions (Coradi et al., 2020). The control interventions are used to maintain the moisture content around the recommended value, which is around 14 per cent for maize grains. Existing grain monitoring methods involve periodic manual measurements of small representative grain samples from different areas of large storage. Other methods involve dividing the storage into layers and estimating the MC values for each layer (Lutz & Coradi, 2022). Since the distribution of moisture in the silo/bin is uneven, such MC measurement by providing the estimated MC value of the grain sample cannot show the exact locations in the bin which are prone to spoilage (Azmi et al., 2021). Methods that show the spatial distribution of moisture in the bin/silo are desirable for efficient monitoring. Such methods can be achieved through electromagnetic imaging techniques, among other methods.

Electromagnetic imaging (EMI) can provide a spatial distribution of the electrical properties of grain throughout the storage bin. The EMI has been applied widely in many fields, such as medical imaging (Aby & Maier, 2020; LoVetri et al., 2020), through-the-wall radar imaging (TWRI) technologies (Mkemwa et al., 2023) and tomography (Mwambela, 2023). In grain monitoring, the EMI technique can provide spatial distribution images that carry qualitative and quantitative information such as physical properties, shape, location, and the extent of the grain conditions. All that information with relatively high spatial resolution is obtained without disturbing or interacting with the grain.

Most EMI applications employ the same operating processes, i.e., field measurements and image reconstruction. However, the EMI technologies differ in sensing techniques,

sensor electronics, measurement procedures, image reconstruction algorithms, and types of electromagnetic waves (Mwambela, 2023; Mwisomba et al., 2022). Unlike other EMI technologies, which use hard-field waves, Electrical capacitance tomography (ECT) uses non-penetrating and bending soft-field electromagnetic waves, which are safe (Chowdhury et al., 2022). The ECT systems use relatively low-frequency electrical fields and cheap capacitance plates as transmitters and receivers. The existing study for monitoring grains MC using imaging technologies involves hard-field electromagnetic waves (Asefi et al., 2016; Asefi et al., 2017). The ECT system is much cheaper than other imaging methods, making it suitable for grain MC monitoring applications (Chowdhury et al., 2022).

In this study, the ECT system was calibrated against the oven-drying method to derive equations correlating MC with output voltages. In calibrating the system for imaging, the Perspex materials of known shapes and spatial distribution were used. Then, the system was adapted for visualizing the moisture contents in the grain using the maize samples with predetermined MC levels. Additionally, in all considered imaging cases, two versions of Linear Back Projection (LBP) image reconstruction algorithms were employed. The results demonstrated that the ECT system successfully generated clear images of the Perspex shapes and accurately depicted the MC distribution within the grains in the sensing area.

Section 2 presents materials and methods that provide an overview of ECT systems. Then, it presents methods for calibrating the ECT system for moisture content measurements and imaging. Materials used for calibration, including the Perspex material, the ECT sensor and the grain samples, have been presented. Section 3 presents the results, including the results for system calibration for MC measurement, imaging the Perspex material and imaging spatial MC distribution in the grain samples. Section 4 presents the conclusion and provides recommendations

for further improvements.

MATERIALS AND METHODS

The ECT System

A basic capacitance-based tomographic imaging system consists of three major parts: a sensing unit, a sensor electronic unit, and an imaging unit (George et al., 2024). The sensing unit consists of electrode plates surrounding the sensing area where the material to be imaged is placed. The capacitance (plate) electrodes are symmetrically mounted outside an insulating pipe wall or vessel. The pipe wall is made of insulating material, which protects the plate electrodes from contact with the measured materials, thus making ECT a non-invasive and non-intrusive technique. The shape and number of electrodes of the ECT sensor differs depending on the applications. The number of electrodes for most sensors is 6, 8, 12, or more (Ahmed Ghaly et al., 2023; Shen et al., 2020). The large number of electrodes increases image quality at the cost of increased measurement time and image reconstruction time.

The sensor electronic unit converts capacitances to voltages, takes measurements using the ECT measurement principles, and conveys information to the imaging unit. The capacitance measurements principle usually involves a single electrode excitation scheme (Hampel et al., 2022; Wang et al., 2021).

With reference to Figure 2a, consider the sensor with n electrodes, mutual capacitances are determined by applying the excitation voltage to electrode E_1 while keeping all others at ground and capacitances between electrodes E_1 and E_2 to E_n are measured; next, the excitation voltage is applied to the electrode E_2 and the capacitance between the electrodes E_2 and E_3 to E_n are measured, and this procedure is repeated until the voltage is applied to the electrode E_{n-1} and the capacitance between the electrodes E_{n-1} and E_n is measured. Therefore, the number of independent measurements is given by (1), with only $\frac{n}{2}$ unique measurements. For the 8-electrode sensor, 28 independent capacitance measurements are obtained, and the overall interrogation of the sensor cross-section is shown in Figure 2a.

$$M = \frac{n(n-1)}{2} \quad (1)$$

The imaging unit implements various image reconstruction algorithms to produce the spatial distribution images of materials in the sensing unit (Mwambela, 2023). The reconstruction algorithms use the capacitance measurements and sensitivity matrix of the sensing area to produce images. The sensitivity matrix is obtained by dividing the sensing area into N elements or pixels, which can be 800, 900, or 1024.

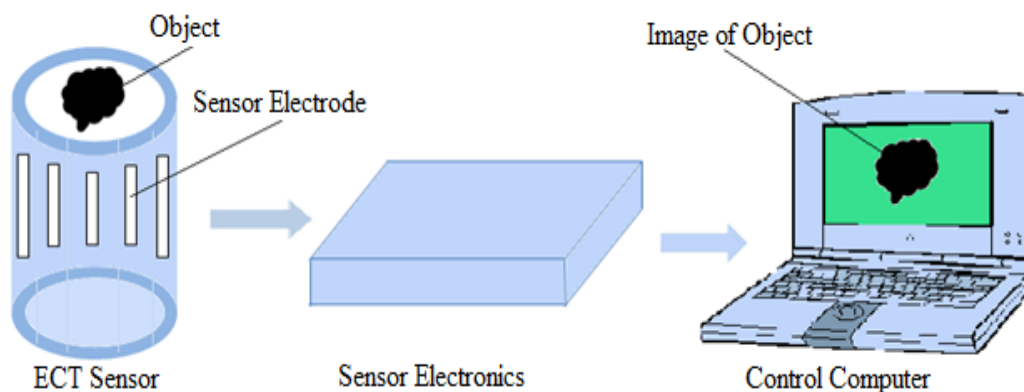


Figure 1: Basic Parts of ECT Measurement System.

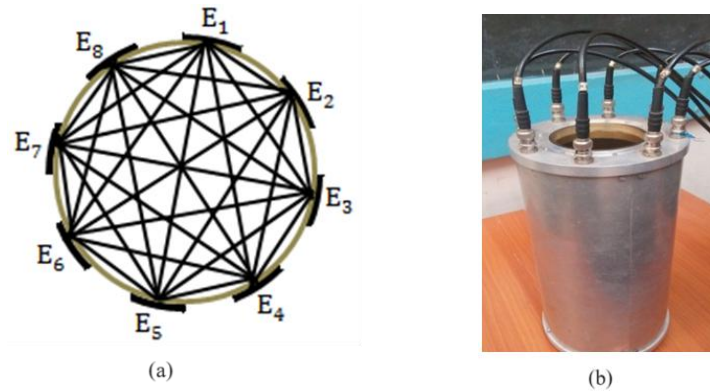


Figure 2: The ECT sensor (a) Sensor interrogation for a single electrode excitation scheme, (b) Practical eight-electrodes ECT sensor.

With assumptions that $M \ll N$, The ECT image reconstruction problem is usually linearized, discretized to matrix form, and written as a normalized vector given by (2).

$$\lambda = Sg \quad (2)$$

Where λ is $M \times 1$ normalized capacitance vector, S is $M \times N$ sensitivity matrix, g is $N \times 1$ normalized permittivity vector, i.e. the grey level of pixels for visualization.

The sensitivity matrix S is dependent on the material to be measured and generated using Finite Element Methods (FEM) (Wahab, 2020). The normalized capacitance vector λ is usually obtained from field measurement data. Therefore, the major task of image reconstruction algorithms is to determine the unknown g from known λ and S as presented in (3) (Gebhardt & Scheinert, 2011).

$$g = S^{-1}\lambda \quad (3)$$

The matrix S is rectangular, its inverse does not exist. One of the key features that differentiates image reconstruction algorithms is the technique they use to find the inverse of a matrix S . Therefore, iterative and non-iterative algorithms have been proposed to solve image reconstruction problems in ECT. Iterative algorithms offer good image quality but demand intensive computations, so they are time-consuming. Non-iterative algorithms are fast and simple to implement (Nombo et al., 2021). Linear Back Projection (LBP) is a typical example of a non-iterative algorithm. The LBP

replaces the inverse of S by its transpose as presented in (4).

$$g = S^T\lambda \quad (4)$$

The LBP is one of the simplest and fastest reconstruction algorithms in the ECT. Several studies have proposed the improvement of LBP. The most popular technique to improve LBP is truncation mechanisms that limit the grey values within the required range, between 0 and 1. A simple truncation mechanism (LBP-Simple) traverses all the grey levels, assigns the grey value 1 to all values greater than 1 and assigns 0 to all values less than 0. Another truncation mechanism is explained by Xie, which can be referred to as LBP-Xie (Mwambela, 1999). In this study, the LBP-Simple and LBP-Xie were used to reconstruct the spatial distribution of MC in the grain.

The practical ECT sensor

The ECT sensor in Figure 2 (b) was used as a container for grain under investigation. The sensor is cylindrical, 30 cm high, and has a circular cross-section with a sensing radius of about 8 cm. Eight identical electrodes surround the sensing area; each electrode has a height of 10 cm and a width of 2.5 cm. The ECT sensor, primarily modelled by FEM for two-component distribution measurements, and its associated sensitivity map was used.

Implementation of ECT system for imaging spatial MC distribution

The implementation involved three main steps, as presented in Figure 3. Firstly, the system was calibrated for moisture content measurement to get the relationship between the readings of the ECT system and moisture contents. Secondly, the system was calibrated to evaluate the ECT system's effectiveness in visualizing the spatial distribution of contents, utilizing simulated distribution data from Perspex as a reference for comparison. Perspex was chosen due to its dielectric constant being similar to that of dry grains. Thirdly, the system was tested for imaging the distribution of moisture content in the grain samples.

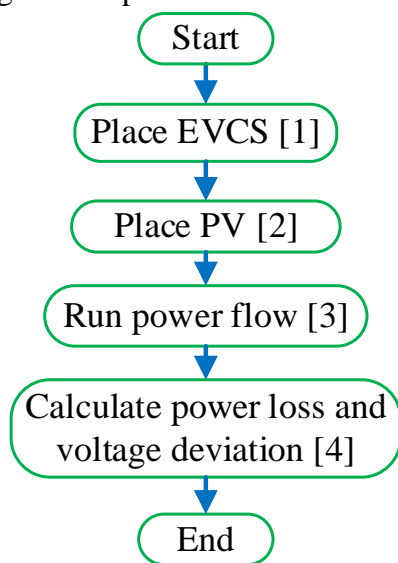


Figure 3: Procedures for implementing ECT system for MC measurement.

System calibration for measurements of MC in grains

In establishing the relationship between the MC and the readings of the ECT system the oven method was used as a reference point. The oven method is one of the most common laboratory-based methods for grain MC measurement. With the oven method, considering the wet basis technique, the water content is calculated from the difference in the grain sample weight before and after drying, as presented in (5) (Bala, 2016).

$$\% \text{ Water Content} = \frac{\text{Measured Weight} - \text{Dry Weight}}{\text{Initial weight}} \times 100\% \quad (5)$$

The dry weight is the weight of the grain sample without moisture content. The initial weight is the weight of the grain sample with the maximum moisture content. The measured weight is the weight of a grain sample at any instant. Figure 4 presents the experimental procedures for calibrating the ECT system for measuring the MC contents in the grains. Firstly, the grain sample with a specific moisture value is measured using the ECT system in order to get its corresponding voltage values. Then, the weight of the same sample is measured in order to get its corresponding weight which will be used to calculate the MC contents using (5). Then, the sample is dried in the oven in order to change the moisture content value. The current MC reading is compared with the previous reading in order to observe the weight changes. When there is no weight change between consecutive readings after drying, the sample is considered totally dry and the procedure stops. The weight of the dry sample is used as a reference point for calculating the water content in the previous measurements, and therefore, the relationship between water content and voltage readings of the ECT system is obtained.

System calibration for imaging the spatial distribution

The ECT system was calibrated for imaging the spatial distribution of contents using Perspex materials with known shapes and permittivity. The main idea was to compare the shape produced by the ECT system and the actual shape of Perspex material. Referring to Figure 5, the second from the right is a phantom with a small hole at the centre (Annular 1), and the second from the left is a phantom with a large hole (Annular 2). The first phantom from the right is a phantom filling half of the sensor cross-section (Stratified).

Since the system was designed for a two-phase flow regime, the first phantom from the left provided capacitance measurement for full-filled sensors. The capacitance measurements of air were taken when the sensor was empty. According to ECT

measurement and imaging principles, the full and empty sensor measurements were used as reference values for normalizing measurement data. Then, the measurement is taken according to the ECT measurement procedures as presented in Section 2.1. With

the sensor of eight electrodes, twenty-eight measurements of each set were obtained. Then, from the full and empty reference measurements, the images of the measured materials were produced using the ECT image reconstruction algorithms.

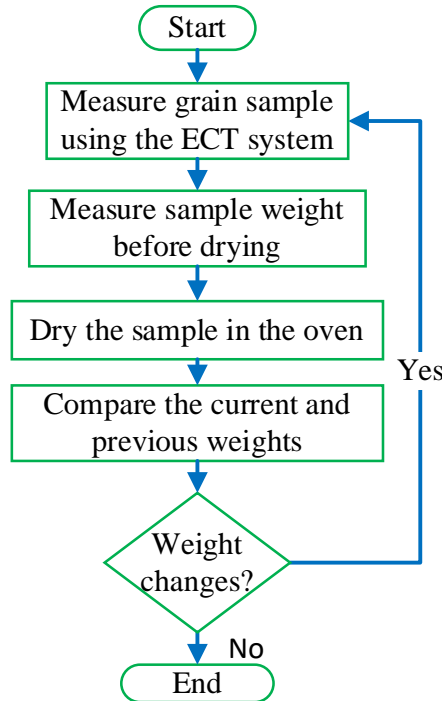


Figure 4: A flowchart for ECT system calibration for MC measurement



Figure 5: Phantoms of Perspex Material, (a) Full Cross Section (b) Large Annular Ring of PM (c) Small Annular Ring of PM (d) Half Cross Section (Stratified)

Imaging spatial distribution of moisture contents in grains

In this study, maize grain was used to test the application of the proposed ECT system in determining the spatial distribution of MCs in the grains. The dielectric constant of dry grain ranges between 2 and 3, and the dielectric constant of water is around 80. Therefore, maize samples with different MC have different permittivity values (Funk et

al., 2004). The ECT employs that permittivity difference to image the spatial distribution of MC in the grain sample. In maintaining the hygroscopic balance in grain samples, the recommended moisture value for maize grain is 14%. Therefore, two samples were used, one with a moisture value above the recommended (20%, a wet sample) and another with a moisture value just below the recommended value (12%, a

dry sample). The wet and dry samples were used to get maximum and minimum reference values for normalizing measurement data as per the requirements of ECT principles. The same samples were put together in the sensor, with one portion filled with a dry sample and another portion with a wet sample (Stratified). To get Annular shapes, the wet maize grains were made to surround the dry maize grains and vice versa. The ratio of wet and dry samples in the sensor was changed to get different Stratified and Annular distributions.

RESULTS AND DISCUSSION

ECT system calibration results for MC measurements

The calibration procedures were performed to establish the reference moisture measurements and their corresponding electrical measurements of the ECT system. The maize sample with an initial weight of 1285.2g was considered. Several measurements were taken until there were no significant weight changes between subsequent measurements. The final weight

of the sample was 1023.4g. This sample was considered a reference dry sample.

Table 1 presents the voltage readings of the ECT system for four electrode pairs alongside the corresponding grain weights. Based on these results, equations were developed to establish the relationship between moisture content and the output voltage of the ECT system for each electrode pair. Given the scattered nature of the data, linear regression was employed to approximate these equations, which are essential for estimating the sample's moisture content from the ECT system's voltage readings. For brevity, the graphical representation is provided for electrode pairs E_{13} and E_{14} as presented in Figure 6.

The estimated equations for electrode pairs E_{13} and E_{14} are provided in Equations (6) and (7), respectively. Using these equations and the proposed ECT system, the moisture content of grain samples can be determined from the system's voltage output using any of the electrode pairs. Among these, electrode pair E_{14} is preferred for moisture content estimation due to its superior stability and linearity.

Table 1 ECT System Calibration Results

Measurement	$E_{12}(V)$	$E_{13}(V)$	$E_{14}(V)$	$E_{15}(V)$	Measured Weight (g)	Water Content (g)	Water Content (%)
1	1.86739	0.96763	0.85169	0.88165	1285.2	261.8	20.37
2	1.85548	0.95429	0.82123	0.81367	1266.6	243.2	19.20
3	1.87194	0.93461	0.81111	0.74927	1238.8	215.4	17.39
4	1.84636	0.94876	0.79343	0.73200	1210.4	187.0	15.45
5	1.86868	0.86209	0.72548	0.68346	1174.3	150.9	12.85
6	1.84728	0.85743	0.70819	0.66440	1138.3	114.9	10.09
7	1.78217	0.80012	0.66487	0.62356	1102.5	079.1	07.17
8	1.77833	0.78234	0.64348	0.62012	1075.4	052.0	04.84
9	1.75023	0.76782	0.63507	0.61863	1042.1	018.7	01.79
10	1.72454	0.75274	0.63106	0.61928	1023.4	000.0	00.00

$$\% MC_{13} = 85.047 \times Voltage - 62.462 \tag{6}$$

$$\%MC_{14} = 84.089 \times \text{Voltage} - 50.348 \quad (7)$$

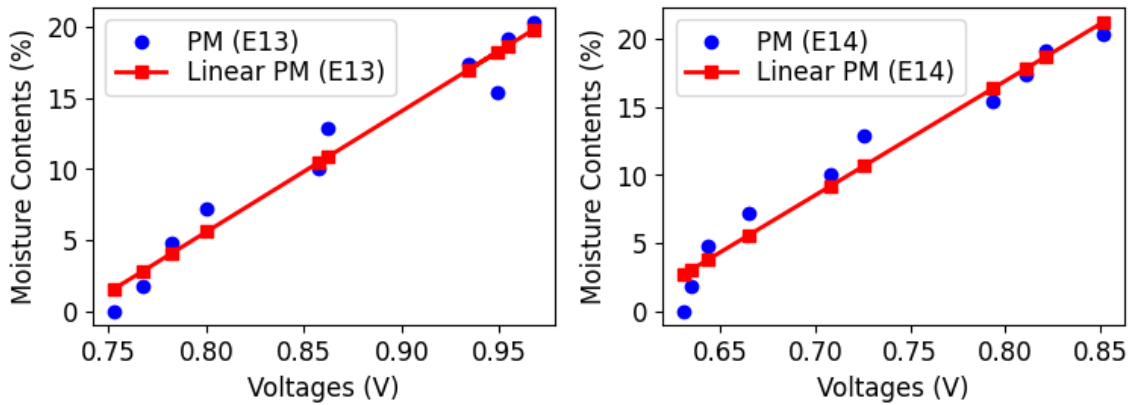


Figure 6: Calibration results for electrode pairs E_{13} and E_{14} .

Table 2: Image reconstructed for Perspex phantoms

		Annular 1	Annular 2	Stratified
Reference distribution images				
Images from simulated capacitances	LBP-Simple			
	LBP-Xie			
Images from measured capacitances	LBP-Simple			
	LBP-Xie			

ECT system calibration results for imaging spatial distribution

In the first experiment, the proposed system was used to image the distribution of Perspex material in the sensor. Perspex materials of different shapes, as presented in Figure 3, were used. Two image reconstruction algorithms, namely LBP-SIMPLE and LBP-XIE, were used. The comparison involved the data obtained from model simulation, which is considered the reference for comparing the performances of algorithms. The algorithms were used to reconstruct

images from simulated capacitances and capacitance measured by the proposed system, as presented in Table 2.

Consider Table 2; when comparing measured and simulated images, all the image reconstruction algorithms LBP-SIMPLE and LBP-XIE could depict the shape of the material in the sensor. However, the LBP-XIE produces better images than the LBP-SIMPLE. Similarly, considering individual algorithms, results for simulated and measured images are almost similar. The results imply that the proposed system can provide good images that are very close to the

simulated images. Another comparison was made involving the Correlation Coefficient (CC) between reconstructed images from simulated and measured capacitances, as presented in Table 3. The results for all algorithms show a very high correlation coefficient, which implies the effectiveness of the proposed system in imaging the material distribution.

Results for imaging spatial distribution of moisture contents in grains

In imaging the spatial distribution of MC in grains, two maize samples with different

moisture content (MC) levels were prepared, and their MC was determined using Equations (6) and (7). The first sample had an MC of 12% and was classified as dry (low permittivity constant), while the second had an MC of 20% and was classified as wet (high permittivity constant). The samples were arranged within the sensor to form stratified, annular 1, and annular 2 shapes, allowing comparisons with earlier analyses using Perspex material. They were then configured into additional shapes representative of real-world grain storage scenarios to ensure practical applicability.

Table 3: The Correlation Coefficient of images from Measured and Simulated Capacitance

	Annular 1	Annular 2	Stratified
LBP-Simple	98.38	98.57	96.13
LBP-Xie	98.38	97.66	93.29

Table 4: Images for Distribution of Moisture Content in Maize

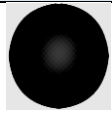
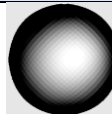
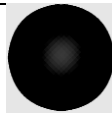
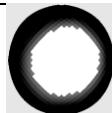
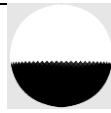
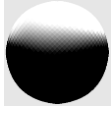
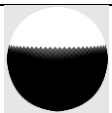
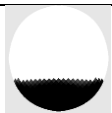
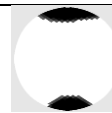
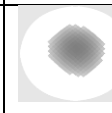
		Annular 1	Annular 2	Stratified
Reconstructed Distribution of Maize	LBP-Simple			
	LBP-Xie			

Table 5: Other Images for Distribution of Moisture Content in Maize

		Shape 1	Shape 2	Shape 3	Shape 4
Others Reconstructed Distributions of Maize	LBP-Simple				
	LBP-Xie				

The annular 1 shape was created by placing a small sample of dry maize at the center, surrounded by a larger sample of wet maize. Conversely, the annular 2 shape consisted of a large dry maize sample at the center, encircled by a smaller wet maize sample. The stratified shape was formed by arranging equal-sized samples of wet and dry maize

side by side. Additional shapes were also tested:

- **Shape 1:** A large wet maize sample occupied approximately three-quarters of the sensor volume, with dry maize filling the remaining one-quarter.
- **Shape 2:** A large dry maize sample covered about three-quarters of the

sensor volume, with wet maize occupying one-quarter.

- **Shape 3:** A dry maize sample was placed at the centre, flanked by wet maize samples on both sides, representing a typical case of moisture content build-up from the outer to the inner regions.
- **Shape 4:** A wet maize sample was positioned at the centre, surrounded by dry maize.

The spatial distribution of moisture content for these configurations is detailed in Tables 4 and 5. The results indicate that the proposed ECT system successfully generated images representing the moisture content distribution for most shapes and across all algorithms considered. However, discrepancies were observed between algorithms, with images produced by LBP-XIE being clearer than those from LBP-SIMPLE.

The images of Annular 1 (Table 4) and Shape 4 (Table 5) are less distinct at the center, highlighting inherent limitations of the ECT system and its reconstruction algorithms in accurately detecting moisture content at the center of the sensing volume. Consequently, identifying moisture content originating from the center is challenging with the current system.

Nevertheless, as noted by Magan and Aldred (2007) initial grain spoilage in storage systems typically occurs near the walls rather than at the centre. The images for Shape 3 (Table 5) are notably clear, demonstrating the system's effectiveness in capturing the common spoilage scenario that originates near the walls. This result reinforces the viability of the proposed ECT system as a practical solution for monitoring grain moisture content and addressing real-world grain storage challenges.

CONCLUSIONS AND RECOMMENDATIONS

The application of Electrical Capacitance Tomography (ECT) for imaging the spatial distribution of moisture content in grain was explored in this study. The ECT system was developed and calibrated to measure grain

moisture content effectively. To evaluate its imaging capabilities, Perspex material with a known permittivity constant and shape was used as a reference. Subsequently, maize samples with varying moisture contents were placed in the sensor to simulate different moisture distribution scenarios. Two image reconstruction algorithms, LBP-SIMPLE and LBP-XIE, were employed in the analysis. The results demonstrated that the ECT system successfully generated clear images of the known Perspex shapes and accurately visualized the spatial distribution of moisture content in the maize samples.

The findings demonstrate that the ECT system can successfully image the spatial distribution of moisture content in grain samples. However, limitations in image resolution, particularly near the center of the sensor, stem from inherent characteristics of the ECT system and its associated image reconstruction algorithms. Future research could address this by testing existing reconstruction algorithms or developing new algorithms specifically tailored for moisture content monitoring.

A circular sensing area with an approximate radius of 8 cm was used. Expanding the sensing area or exploring alternative sensor geometries, such as square-shaped sensors, could enhance the system's versatility. Additionally, while the images were presented in 2D, which provides a cross-sectional view of the sensing area, incorporating 3D imaging techniques could offer a more comprehensive representation of moisture distribution. Finally, while this study focused on imaging defined shapes of moisture content distributions to validate the concept, future work could explore more complex and varied spatial distribution patterns to evaluate the system's practical applicability in real-world scenarios.

REFERENCES

- Aby, R. G., & Maier, D. E. (2020). Advances in techniques for monitoring the quality of stored cereal grains. In *Advances in postharvest management of cereals and*

- grains (pp. 363-388). Burleigh Dodds Science Publishing.
- Ahmed Ghaly, S. M., Khan, M. O., Shalaby, M., Al-Snaie, K. A., Ali, M. A., Faisal, B., Imad, A., & Oraiqat, M. (2023). Electrical Capacitance Tomography-Based Flow Measurement in a Closed Container Using 16-Electrode Sensor in Contrast with 8-Pair-16-Electrodes Topology. *Journal of Nanoelectronics and Optoelectronics*, **18**(5), 611-618. doi: 10.1166/jno.2023.3427
- Asefi, M., Faucher, G., & LoVetri, J. (2016). Surface-current measurements as data for electromagnetic imaging within metallic enclosures. *IEEE Transactions on Microwave Theory and Techniques*, **64**(11), 4039-4047. doi: 10.1109/TMTT.2016.2605665
- Asefi, M., Gilmore, C., Jeffrey, I., LoVetri, J., & Paliwal, J. (2017). Detection and continuous monitoring of localised high-moisture regions in a full-scale grain storage bin using electromagnetic imaging. *Biosystems engineering*, **163**, 37-49. doi: [10.1016/j.biosystemseng.2017.08.015](https://doi.org/10.1016/j.biosystemseng.2017.08.015)
- Azmi, N., Kamarudin, L. M., Zakaria, A., Ndzi, D. L., Rahiman, M. H. F., Zakaria, S. M. M. S., & Mohamed, L. (2021). RF-based moisture content determination in rice using machine learning techniques. *Sensors*, **21**(5), 1875. doi: [10.3390/s21051875](https://doi.org/10.3390/s21051875)
- Bala, B. K. (2016). *Drying and storage of cereal grains*. John Wiley & Sons: New York, NY, USA.
- Chowdhury, S. M., Marashdeh, Q., Teixeira, F. L., & Fan, L.-S. (2022). Electrical capacitance tomography. In *Industrial Tomography: Systems and Applications*, 2nd ed.; Wang, M., Ed.; Woodhead/Elsevier: Cambridge, UK, Chapter 1; pp. 3–29. doi: [10.1016/B978-0-12-823015-2.00002-9](https://doi.org/10.1016/B978-0-12-823015-2.00002-9)
- Coradi, P. C., Maldaner, V., Lutz, É., da Silva Daí, P. V., & Teodoro, P. E. (2020). Influences of drying temperature and storage conditions for preserving the quality of maize postharvest on laboratory and field scales. *Scientific reports*, **10**(1), 22006. doi: 10.1038/s41598-020-78914-x
- Fu, J., Yue, X., Zhang, Q., & Li, P. (2024). Early warning technologies for mycotoxins in grains and oilseeds: A review. *Trends in Food Science & Technology*, 104479. doi: [10.1016/j.tifs.2024.104479](https://doi.org/10.1016/j.tifs.2024.104479)
- Funk, D., Meszaros, P., Gillay, Z., Rampton, J., & Freese, L. (2004). *New Dielectric Moisture Measurement Technologies 2004 International Quality Grains Conference Proceedings*, Indianapolis, Indiana, USA.
- Gebhardt, S., & Scheinert, G. (2011). Position determination based on electrical capacitance tomography. *COMPEL: The International Journal for Computation and Mathematics in Electrical and Electronic Engineering*, **30**(4), 1224-1236. doi: [10.1108/03321641111133145](https://doi.org/10.1108/03321641111133145)
- George, N., Ally, N., & Nombo, J. (2024). Diffusion-Steered Algorithm for Improving Quality of Images Generated by Electrical Capacitance Tomography Measurement System. *Tanzania Journal of Science*, **50**(2), 387-396. doi: 10.4314/tjs.v50i2.17
- Hampel, U., Babout, L., Banasiak, R., Schleicher, E., Soleimani, M., Wondrak, T., Vauhkonen, M., Lähivaara, T., Tan, C., & Hoyle, B. (2022). A review on fast tomographic imaging techniques and their potential application in industrial process control. *Sensors*, **22**(6), 2309. doi: [10.3390/s22062309](https://doi.org/10.3390/s22062309)
- Leal, M. M., Rodrigues, D. M., de Moraes, R. S., Jaques, L. B. A., da Silva Timm, N., & Coradi, P. C. (2023). Monitoring of intergranular variables for predicting technical breakage of wheat grains stored in vertical silos. *Journal of Stored Products Research*, **102**, 102115. doi: [10.1016/j.jspr.2023.102115](https://doi.org/10.1016/j.jspr.2023.102115)
- LoVetri, J., Asefi, M., Gilmore, C., & Jeffrey, I. (2020). Innovations in electromagnetic imaging technology: The stored-grain-monitoring case. *IEEE Antennas and Propagation Magazine*, **62**(5), 33-42. doi: 10.1109/MAP.2020.3003206
- Lutz, É., & Coradi, P. C. (2022). Applications of new technologies for monitoring and predicting grains quality stored: Sensors, internet of things, and artificial intelligence. *Measurement*, **188**, 110609.

- doi:
[10.1016/j.measurement.2021.110609](https://doi.org/10.1016/j.measurement.2021.110609)
- Magan, N., & Aldred, D. (2007). Post-harvest control strategies: minimizing mycotoxins in the food chain. *International journal of food microbiology*, **119**(1-2), 131-139. doi: [10.1016/j.ijfoodmicro.2007.07.034](https://doi.org/10.1016/j.ijfoodmicro.2007.07.034)
- Mkemwa, F., Abdalla, A. T., Maiseli, B., Amour, I., & Muqaibel, A. (2023). Effective path-loss compensation model based on multipath exploitation for through-the-wall radar imaging. *EURASIP Journal on Advances in Signal Processing*, **2023**(1), 42. doi: 10.1186/s13634-023-01004-3
- Mwambela, A. J. (1999). *Reconstruction of Capacitance Data Using Entropic Thresholding Techniques. Ph.D Thesis, University of Dar es salaam, Tanzania.*
- Mwambela, A. J. (2023). Evaluation of Image Enhancement Techniques for Electrical Capacitance Tomography Applications. *Tanzania Journal of Science*, **49**(1), 116-129. doi: 10.4314/tjs.v49i1.11
- Mwisomba, C., Abdalla, A. T., Amour, I., Mkemwa, F., & Maiseli, B. (2022). Fast sparse image reconstruction method in through-the-wall radars using limited memory Broyden–Fletcher–Goldfarb–Shanno algorithm. *International Journal of Microwave and Wireless Technologies*, **14**(6), 739-749. doi:10.1017/S1759078721000866
- Nombo, J., Mwambela, A., & Kisngiri, M. (2021). Analysis and Performance Evaluation of Entropic Thresholding Image Processing Techniques for Electrical Capacitance Tomography Measurement System. *Tanzania Journal of Science*, **47**(3), 928-942. doi: 10.4314/tjs.v47i3.5
- Shen, J., Meng, S., Ye, M., Yang, W., & Liu, Z. (2020). 3D image reconstruction using an ECT sensor with a single layer of electrodes. *Measurement Science and Technology*, **31**(8), 085106. doi: 10.1088/1361-6501/ab82c0
- Wahab, Y. A. (2020). A Simulation Study of Sensor Behavior for Non-Invasive Electrical Resistance Tomography. *Journal of Tomography System and Sensor Application*, **3**(1).
- Wang, W., Zhao, K., Zhang, P., Bao, J., & Xue, S. (2021). Application of three self-developed ECT sensors for monitoring the moisture content in sand and mortar. *Construction and Building Materials*, **267**, 121008. doi: [10.1016/j.conbuildmat.2020.121008](https://doi.org/10.1016/j.conbuildmat.2020.121008)